IEEE Photonics Journal
An IEEE Photonics Society Publication

Open Access

Multilevel Intensity Modulations for Simplified Full-Duplex Millimeter-Wave Radio-Over-Fiber System for Gigabit Access

Volume 4, Number 5, October 2012

A. H. M. Razibul Islam
Masuduzzaman Bakaul
Ampalavanapillai Nirmalathas

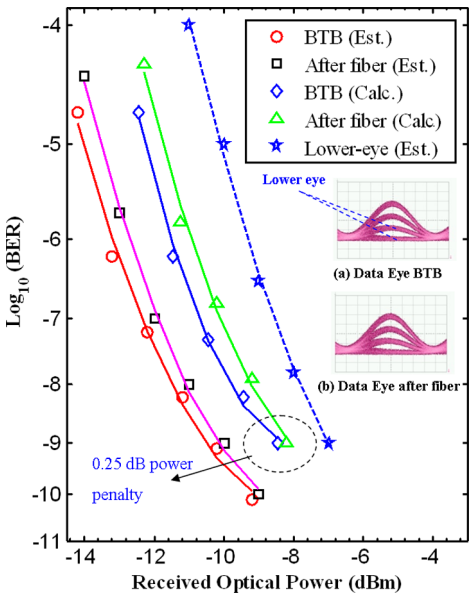

DOI: 10.1109/JPHOT.2012.2220758
1943-0655/$31.00 ©2012 IEEE

IEEE photonics SOCIETY

IEEE

Multilevel Intensity Modulations for Simplified Full-Duplex Millimeter-Wave Radio-Over-Fiber System for Gigabit Access

A. H. M. Razibul Islam,[1,2] Masuduzzaman Bakaul,[1,2] and Ampalavanapillai Nirmalathas[1]

[1]Department of Electrical & Electronic Engineering, University of Melbourne, Parkville, Vic-3010, Australia
[2]NICTA (National ICT Australia Ltd.), Department of Electrical & Electronic Engineering, University of Melbourne, Parkville, Vic-3010, Australia

DOI: 10.1109/JPHOT.2012.2220758

Manuscript received August 24, 2012; revised September 20, 2012; accepted September 20, 2012. Date of publication September 27, 2012; date of current version October 4, 2012. This work was supported by the National ICT Victoria, Australia, funded by the Australian Government as represented by the Department of Broadband, Communications, and the Digital Economy and the Australian Research Council through the ICT Centre of Excellence program. Corresponding author: A. H. M. Razibul Islam (e-mail: aislam@ee.unimelb.edu.au).

Abstract: Multilevel M-ary amplitude-shift-key (M-ASK) intensity modulation formats have been proposed and experimentally demonstrated in millimeter-wave radio-over-fiber (mm-wave RoF) system. In order to demonstrate multilevel intensity modulation for spectrally efficient implementation, return-to-zero (RZ) and non-RZ (NRZ) implementations for both 4-ASK and 8-ASK modulation formats are utilized in full-duplex RoF link. Hence, for downlink, two different signal generation schemes are utilized in this paper for optical mm-wave generation and transport using optical heterodyning of two unlocked lasers. For uplink, similar RF self-homodyning technique is applied at the base station (BS) to simplify the signal translation process. Theoretical analyses and experimental results using the proposed technique for M-ASK modulation formats confirm the system's performance. Apart from the bandwidth-efficient realization of the proposed schemes, demonstrated full-duplex RoF techniques avoid most of the high-speed electrooptic and RF devices from both the central station (CS) and BSs keeping the optical mm-wave generation, optical transport, and BSs simpler in both directions.

Index Terms: Fiber optics systems, heterodyning, homodyning, multilevel modulation, radio over fiber (RoF), microwave photonics.

1. Introduction

Future broadband wireless access (BWA) and backhaul systems need to support multigigabit bandwidth-intensive applications as bandwidth demands are increasing at the consumer level. Due to the limited available bandwidth and congested lower microwave frequencies (< 5 GHz), current wireless networks need to operate at higher frequency regions to address future aggregate bandwidth demands of 10 GHz or higher [1].Therefore, upper frequency windows in the millimeter-wave (mm-wave) regions such as wireless metropolitan area networks at 10–66 GHz, wireless personal area networks at 60 GHz, and E-bands operating at 70, 80, and 90 GHz for BWA services are of particular interest.

In order to exploit the congestion-free spectral domain of these frequency bands, the mm-wave radio over fiber (RoF) is an attractive solution. In a mm-wave RoF system, a low-loss optical fiber link is established to transmit mm-wave signals where central stations (CSs) processes the signal generation, data modulation, upconversion etc., and the base stations (BSs) are distributed through the common fiber network [2]. As the BSs need to transmit the mm-wave signal to the end user, the operational coverage of BSs reduces to pico- or femtocells due to inherent high atmospheric attenuation at mm-wave bands [3]. This translates to a larger number of BS requirements to allocate coverage to the total geographic area. Low-cost optical mm-wave generation, photonic frequency upconversion strategies and efficient modulation formats at the CS are therefore the main drivers for simplified, efficient, and cost-effective distribution of signals to the remote BSs. Minimization of high-speed components from the BS and simpler signal translation schemes play a significant role in this regard to meet the performance-to-cost-ratio requirements.

In our recent demonstrations [4], [5], we proposed and demonstrated mm-wave RoF system where two uncorrelated optical carriers were heterodyned without any phase/frequency locking, and later, the transmitted data was recovered using phase-insensitive incoherent demodulation technique, i.e., RF self-homodyning. Such technique removed any phase/frequency locking, high-speed modulators, and LO at the generation and transport of optical mm-wave signals. Additionally, it avoided high-speed RF devices (i.e., LO) at the BS and relaxed signal translations for both downlink and uplink directions, respectively. Simple modulation scheme such as amplitude-shift-key (ASK) modulation format was chosen in our previous demonstrations [4], [5], although not spectrally efficient. Multilevel intensity modulation, such as multilevel ASK (M-ASK), can be a potential solution in this regard to offer spectrally efficient realization using our proposed technique. Additionally, signal generations can still be simpler, and higher data rates can be supported without adding any complex hardware for signal processing components [6]. Moreover, additional phase component processing of complex modulation schemes such as quadrature amplitude modulation or differential phase-shift keying can be avoided by such proposed upgrade to M-ASK modulation. On the whole, reducing the symbol rate through M-ASK implementations allows cheaper RF and optoelectronic components at the transmitter and receiver while offering reduced hardware complexity due to using incoherent detection at the receiver.

Although there are no current standards on M-ASK-based RoF systems, in this paper, we proposed and introduced 4-ASK and 8-ASK modulation formats to double and triple the data rates, respectively without expanding the spectral width compared with ASK scheme. Both non-return-to-zero (NRZ) and return-to-zero (RZ) data formats were used to demonstrate the system performances experimentally. We considered two signal generation schemes for all RZ and/or NRZ 4-ASK and 8-ASK experiments where both of the lasers are modulated at CS (Scheme A) and one of the lasers is modulated and optically combined with the unmodulated carrier (Scheme B) located at CS. While our previous work in [5] detailed the theoretical descriptions of our proposed technique for ASK-based downlink systems, we extended the analysis for the M-ASK-based downlink and uplink systems in this paper. Apart from that, RZ demonstrations are considered for the first time in our proposed technique for the full-duplex M-ASK implementations as RZ has better noise immunity [7], [8].

Section 2 of the paper describes the conceptual full-duplex system configurations and theoretical analyses of two signal generation schemes termed as Schemes A and B. Full-duplex experimental results for each of the schemes using M-ASK modulation formats are discussed in Section 3. Both downlink and uplink system performances are discussed in Sections 3 and 4. Finally, Section 5 summarizes the concluding remarks of this paper.

2. System Configurations and Theoretical Descriptions

Downlink configurations for optical mm-wave generation and transport using Schemes A and B are shown in Fig. 1(a) and (b), respectively. Fig. 2(a) presents the phase-insensitive RF self-homodyning of data at the downlink receiver common to both Schemes A and B. On the other hand, Fig. 2(b) presents the uplink configurations in all the schemes where the RF self-homodyning is utilized again.

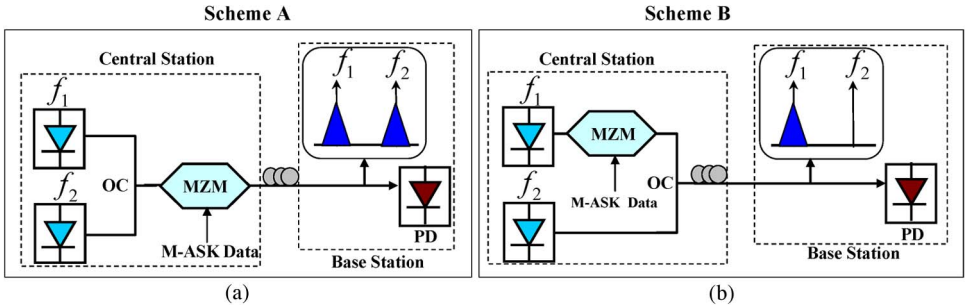

Fig. 1. Signal generation schemes for M-ASK-based mm-wave RoF downlink using (a) Scheme A and (b) Scheme B.

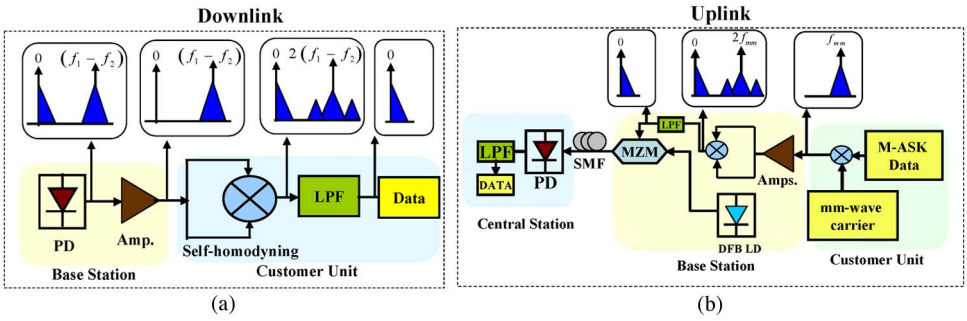

Fig. 2. M-ASK-based mm-wave RoF system configurations for (a) downlink and (b) uplink.

The electric fields of the lasers can be written as:

$$E_1 \exp j(2\pi f_1 t + \phi_1) \tag{1}$$

$$E_2 \exp j(2\pi f_2 t + \phi_2). \tag{2}$$

where E_1 and E_2 are the amplitudes, f_1 and f_2 are the optical frequencies of two lasers, and ϕ_1 and ϕ_2 are the phases of lasers, respectively. In order to simplify, let us assume $E_1 = E_2 = 1$ and the modulating M-ASK signal is sinusoidal, which can be expressed as

$$s(t) = S_i \cos 2\pi f_m t, \quad 0 \le t \le T \tag{3}$$

where $S_i = S[2i - (M-1)]$, $i = 0, 1, \ldots, M-1$, and $M \ge 4$. S is a constant, M is the distinct finite-energy signal levels, f_m is the modulating frequency, and T is the symbol duration.

2.1. Downlink Using Scheme A

According to the downlink transmitter configurations of Scheme A, as shown in Fig. 1(a), both of the optical carriers are modulated at the CS by the M-ASK data. Here, assuming that the modulator is biased at quadrature and the signal strength $S_i \ll 1$, after Taylor series expansion, we can express the modulated optical carriers as:

$$A_1(t) = \exp j(2\pi f_1 t + \phi_1)\left\{1 + \frac{S_i}{2}[\exp(j2\pi f_m t) + \exp(-j2\pi f_m t)]\right\} \tag{4}$$

$$A_2(t) = \exp j(2\pi f_2 t + \phi_2)\left\{1 + \frac{S_i}{2}[\exp(j2\pi f_m t) + \exp(-j2\pi f_m t)]\right\}. \tag{5}$$

Now, the modulated carriers are transported through the single-mode fiber (SMF) before leading to the photodetector (PD). Following steps as detailed in [5], the detected RF signal after the heterodyning at PD can be expressed as

$$\begin{aligned} i_p(t) &= \Re \times \left[(A_{f_1}(t) + A_{f_2}(t)) \times \left(A^*_{f_1}(t) + A^*_{f_2}(t) \right) \right] \\ &= \Re \times \Bigg[2 + S_i^2 + \frac{S_i}{2}\cos\{2\pi f_m t + (\varphi_1 - \varphi_0)\} + \frac{S_i}{2}\cos\{2\pi f_m t + (\varphi_0 - \varphi_2)\} \\ &\quad + \frac{S_i}{2}\cos\{2\pi f_m t + (\varphi'_0 - \varphi'_2)\} + \frac{S_i}{2}\cos\{2\pi f_m t + (\varphi'_1 - \varphi'_0)\} \\ &\quad + \frac{S_i^2}{4}\cos\{2\pi.2 f_m t + (\varphi_1 - \varphi_2)\} + \frac{S_i^2}{4}\cos\{2\pi.2 f_m t + (\varphi'_1 - \varphi'_2)\} \\ &\quad + \cos\{2\pi(f_1 - f_2)t + (\phi_1 - \phi_2) + (\varphi_0 - \varphi'_0)\} \\ &\quad + \frac{S_i^2}{4}\cos\{2\pi(f_1 - f_2)t + (\phi_1 - \phi_2) + (\varphi_1 - \varphi'_1)\} \\ &\quad + \frac{S_i^2}{4}\cos\{2\pi(f_1 - f_2)t + (\phi_1 - \phi_2) + (\varphi_2 - \varphi'_2)\} \\ &\quad + \frac{S_i}{2}\cos\{2\pi[(f_1 - f_2) - f_m]t + (\phi_1 - \phi_2) + (\varphi_0 - \varphi'_1)\} \\ &\quad + \frac{S_i}{2}\cos\{2\pi[(f_1 - f_2) - f_m]t + (\phi_1 - \phi_2) + (\varphi_2 - \varphi'_0)\} \\ &\quad + \frac{S_i}{2}\cos\{2\pi[(f_1 - f_2) + f_m]t + (\phi_1 - \phi_2) + (\varphi_0 - \varphi'_2)\} \\ &\quad + \frac{S_i}{2}\cos\{2\pi[(f_1 - f_2) + f_m]t + (\phi_1 - \phi_2) + (\varphi_1 - \varphi'_0)\} \\ &\quad + \frac{S_i^2}{4}\cos\{2\pi[(f_1 - f_2) + 2f_m]t + (\phi_1 - \phi_2) + (\varphi_1 - \varphi'_2)\} \\ &\quad + \frac{S_i^2}{4}\cos\{2\pi[(f_1 - f_2) - 2f_m]t + (\phi_1 - \phi_2) + (\varphi_2 - \varphi'_1)\} \Bigg]. \end{aligned} \tag{6}$$

Here, $\Re$ is the responsivity of the PD, and $A^*_{f_1}(t)$ and $A^*_{f_2}(t)$ are the complex conjugates of the optical carriers after passing through the SMF. φ_0, φ_1, φ_2 and φ'_0, φ'_1, φ'_2 represent the phase delays of the spectral components due to fiber chromatic dispersion as the signal passes through the SMF.

The last nine terms in (6) represent the detected mm-wave signal at $(f_1 - f_2)$ with its first- and second-order sideband representations. The uncorrelated phase noise $(\phi_1 - \phi_2)$ can be also seen in (6), along with the mm-wave signal due to unlocked heterodyning. DC terms and the harmonics can be filtered out by using a suitable bandpass filter if a high-pass filter with cutoff frequency $f_m > f_c > (|f_1 - f_2| - 2f_m)$ is used. Hence, assuming $\Re = 1$ and fiber chromatic dispersion negligible (i.e., ≈ 0), (6) after the bandpass filtering can now be written as

$$\begin{aligned} i_p(t) = \Bigg[\left(1 + \frac{S_i^2}{2}\right)\cos\{2\pi(f_1 - f_2)t + (\phi_1 - \phi_2)\} + S_i\cos\{2\pi[(f_1 - f_2 \pm f_m]t + (\phi_1 - \phi_2)\} \\ + \frac{S_i^2}{4}\cos\{2\pi[(f_1 - f_2) \pm 2f_m]t + (\phi_1 - \phi_2)\} \Bigg]. \end{aligned} \tag{7}$$

$(S_i^2/4)$ and $(S_i/2)$ terms in (7) can be generalized as $\mathbb{S}$, where it can vary for the values of n within the range of -2 to $+2$. Hence, we can simplify the (7) as

$$\mathbb{S}\cos[2\pi\{(f_1 - f_2) + nf_m\}t + (\phi_1 - \phi_2)]. \tag{8}$$

Finally, following (12)–(14) in [5], baseband M-ASK data are recovered employing the RF self-homodyning followed by a suitable low-pass filter (LPF) [9]–[11].

2.2. Downlink Using Scheme B

For Scheme B, only one carrier at CS is modulated, and the unmodulated carrier is optically combined with the modulated carrier, as shown in the inset in Fig. 1(b). Therefore, similar to (6), detected mm-wave signal after the PD can be expressed as:

$$\begin{aligned} i_p(t) = \Re \times \Bigg[& 2 + \frac{S_i^2}{2} + \frac{S_i}{2}\cos\{2\pi f_m t + (\varphi_1 - \varphi_0)\} + \frac{S_i}{2}\cos\{2\pi f_m t + (\varphi_0 - \varphi_2)\} \\ & + \frac{S_i^2}{4}\cos\{2\pi.2 f_m t + (\varphi_1 - \varphi_2)\} + \cos\{2\pi(f_1 - f_2)t + (\phi_1 - \phi_2) + (\varphi_0 - \varphi_0')\} \\ & + \frac{S_i}{2}\cos\{2\pi[(f_1 - f_2) - f_m]t + (\phi_1 - \phi_2) + (\varphi_2 - \varphi_0')\} \\ & + \frac{S_i}{2}\cos\{2\pi[(f_1 - f_2) + f_m]t + (\phi_1 - \phi_2) + (\varphi_1 - \varphi_0')\}\Bigg]. \end{aligned} \tag{9}$$

The last three terms in (9) are of interest, and applying similar steps as detailed in Section 2.1, phase-insensitive baseband data can be obtained.

2.3. Uplink for Schemes A and B

For the uplink direction using both of Schemes A and B, generated mm-wave carrier from the LO located at the customer unit (CU) will be mixed with the transmitted baseband M-ASK data, as shown in Fig. 1(d). The upconverted signal can be then expressed as

$$C_{UL}(t) = \left[\cos(2\pi f_{LO} t + \phi_{LO}) + \frac{S_i}{2}\{\cos(2\pi f_{LO} t + \phi_{LO} + 2\pi f_m t) + \cos(2\pi f_{LO} t + \phi_{LO} - 2\pi f_m t)\}\right]. \tag{10}$$

Here, f_{LO} and ϕ_{LO} are the mm-wave LO frequency and its phase, respectively. Now, after the band-limited amplifications, (10) will be multiplied by its own due to RF self-homodyning at the BS. Therefore, the signal after the RF self-homodyning can be represented as

$$\begin{aligned} D_{BS} &= C_{UL}(t) * C_{UL}(t) \\ &= \Bigg[\frac{1}{2} + \frac{S_i^2}{4} + \frac{1}{2}\cos 2(2\pi f_{LO} t + \phi_{LO}) + \frac{S_i^2}{8}\cos 2\{2\pi(f_{LO} + f_m)t + \phi_{LO}\} \\ &\quad + \frac{S_i^2}{8}\cos 2\{2\pi(f_{LO} - f_m)t + \phi_{LO}\} + S_i \cos 2\pi f_m t \\ &\quad + \frac{S_i^2}{4}\cos 2.(2\pi f_m t) + \frac{S_i^2}{4}\cos 2.(2\pi f_{LO} t + \phi_{LO}) \\ &\quad + \frac{S_i}{2}\cos\{2.(2\pi f_{LO} t + \phi_{LO}) + 2\pi f_m t\} + \frac{S_i}{2}\cos\{2.(2\pi f_{LO} t + \phi_{LO}) - 2\pi f_m t\}\Bigg]. \end{aligned} \tag{11}$$

Here, the sixth term in (11) is the recovered phase-noise free data after the RF self-homodyning at the BS. The DC terms and the higher-order harmonics in (11) can be neglected by using a suitable LPF. Hence, the recovered data at the BS is modulated externally by an optical carrier transmitted over a length of SMF and is finally detected by a low-speed PD. The detected RF signal after the PD can be written as

$$\begin{aligned} i_{UL} = \Re \times \Bigg[& 1 + \frac{S_i^2}{2} + \frac{S_i}{2}\cos\{2\pi f_m t + (\varphi_0 - \varphi_2)\} + \frac{S_i}{2}\cos\{2\pi f_m t + (\varphi_1 - \varphi_0)\} \\ & + \frac{S_i^2}{4}\cos\{2.2\pi f_m t + (\varphi_1 - \varphi_2)\}\Bigg]. \end{aligned} \tag{12}$$

Similarly, let us assume $\Re = 1$ and the effects of fiber chromatic dispersion is negligible (i.e., ≈ 0) and remove the DC and higher order components by using a suitable LPF. Thus, the recovered

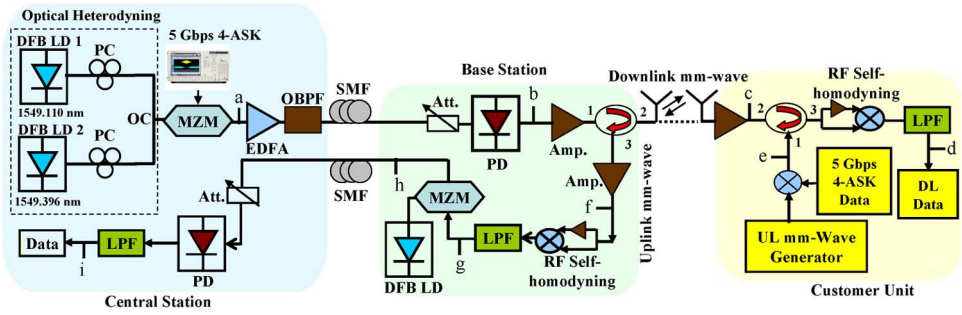

Fig. 3. Full-duplex system configuration for experimental demonstration of Scheme A.

data after the LPF is obtained and can be expressed as

$$i_{UL} = S_i \cos 2\pi f_m t. \tag{13}$$

3. Experimental Setup and Demonstrations

3.1. 4-ASK Demonstrations Using Scheme A

3.1.1. Downlink

Fig. 3 presents the setup for the experimental demonstrations of Scheme A at both downlink and uplink directions. We used two free-running distributed feedback lasers (DFBs) operating at 1549.110 nm and 1549.396 nm, respectively. The lasers were combined using optical coupler (OC) so that an offset mm-wave carrier frequency of 35.75 GHz is maintained. Linewidths of the lasers were 200 kHz and 5 MHz at relative intensity noise of ≤ -145 dBc/Hz each. A *Tektronix* arbitrary waveform generator (AWG) was used to generate the 5-Gb/s 4-ASK data. Both NRZ and RZ formats for the 4-ASK data were generated using the AWG for a data transmission bandwidth of 2.5 GHz. Sampling rates for the NRZ and RZ formats were 2.5 GS/s and 5 GS/s, respectively as the RZ formats need twice the sampling rates than the NRZ formats [12]. We used an LPF of 2.5-GHz bandwidth after the data generation for the NRZ. Due to higher filtering bandwidth requirements for the RZ format, an LPF of 3.8 GHz was used for the same. A Mach–Zehnder modulator (MZM) of 2.5 GHz was used to modulate the generated and filtered data onto the combined optical carriers. The half-wave voltage of the modulator was 2.5 V. The driving RF voltage to the MZM was 1 V peak to peak. As the NRZ format needs higher power than the RZ formats, the bias voltages were 3.5 V and 1.8 V, respectively, for the NRZ and RZ formats. The modulated signal was then optically amplified by an erbium-doped fiber amplifier (EDFA). An optical bandpass filter of 2-nm bandwidth is added after the EDFA to remove the amplified spontaneous emission noise. A high-speed 50-GHz PD was utilized for the remote heterodyne detection of signal after transmission over a SMF span of 25.1 km. The heterodyned signal after the PD contained the phase-noise-embedded modulated mm-wave carrier at the offset carrier frequency of 35.75 GHz, along with its baseband replica. For back-to-back (BTB) wireless transmission, a combination of a low-noise amplifier (LNA) and a medium power amplifier (MPA) at 26.5–40 GHz (Ka band) was then used to provide around $+30$ dB amplification. This band-limited amplification also limits the shot noise, which is introduced by the detection process at the PD, thereby suppressing the baseband replica [13]. The amplified mm-wave signal was then split into two paths by an RF splitter and was led to the RF and LO ports of a Ka-band *Miteq* mixer to perform RF self-homodyning. Sufficient required power at the LO port of the mixer were maintained by amplifying the signal using an LNA. A Ka-band RF phase shifter is utilized before the RF port of the mixer to ensure phase matching of signals in the two split paths. Suitable LPFs of 2.5-GHz and 3.8-GHz bandwidth were used, respectively, to recover the NRZ and RZ 4-ASK formats, which avoid the phase noise due to RF self-homodyning process, as detailed in Section 2.

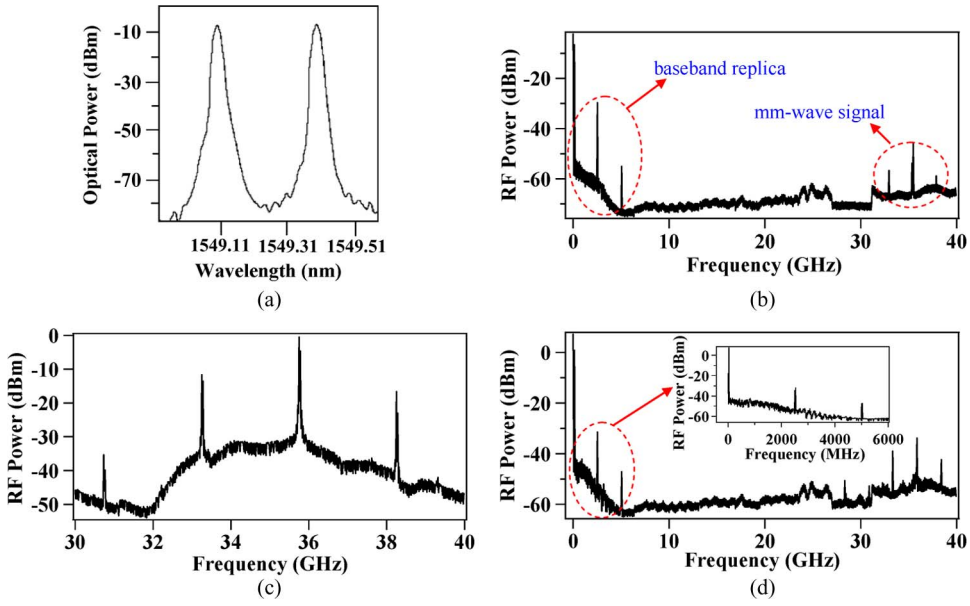

Fig. 4. (a)–(d) presents optical and RF spectra at points a to d of the Scheme A as shown in Fig. 3 using 4-ASK RZ data.

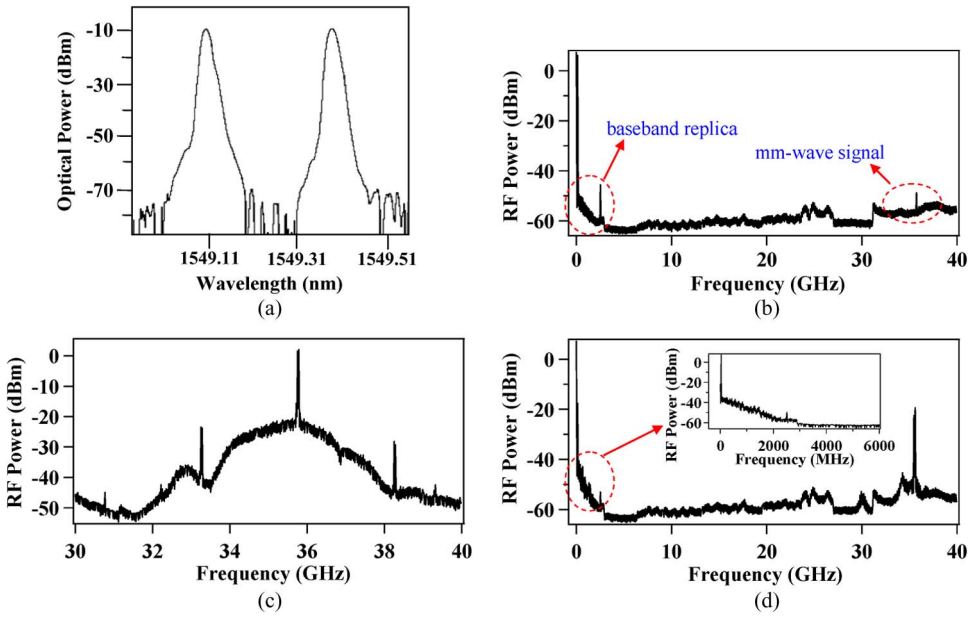

Fig. 5. (a)–(d): Optical and RF spectra at points a to d of the downlink Scheme A as shown in Fig. 3 using 4-ASK NRZ data.

3.1.2. Results and Discussion

In order to investigate Scheme-A system performances, relevant optical and RF spectra for downlink using 4-ASK RZ format are shown in Fig. 4(a)–(d) at points a–d in Fig. 3. The 4-ASK data modulated optical carriers after the MZM are shown in Fig. 4(a). Fig. 4(b) shows the detected modulated mm-wave signal after the PD and its baseband replica. Although the mm-wave signal is

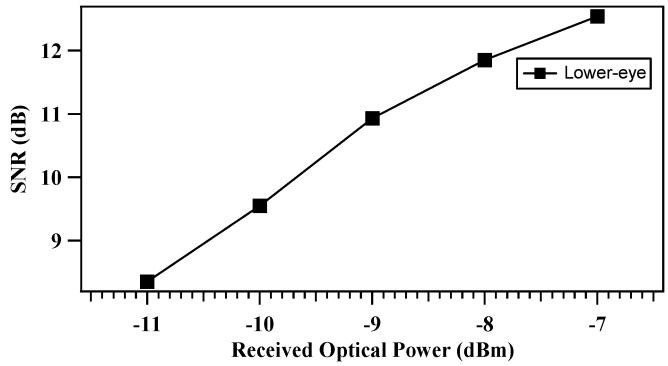

Fig. 6. Estimated SNR of the lower eye for the downlink Scheme A using 4-ASK RZ data.

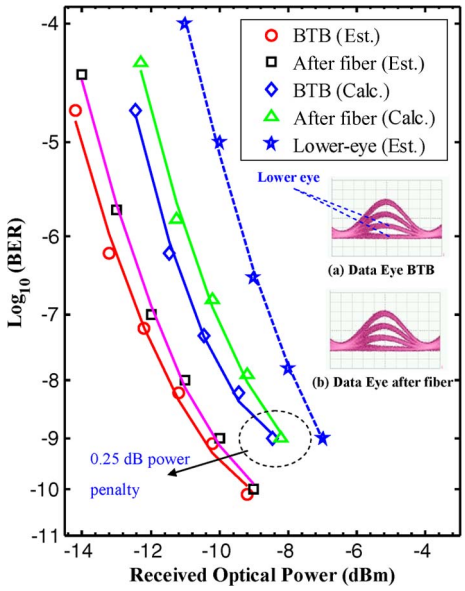

Fig. 7. Downlink BER curves and eye diagrams for scheme A using 4-ASK RZ data.

weak, baseband replica is suppressed after the band-limited amplifications, as shown in Fig. 4(c). Fig. 4(d) shows the recovered 4-ASK RZ data after the RF self-homodyning and filtering. The inset in Fig. 4(d) shows the close-up of the data spectra.

Similar optical and RF spectra for downlink using 4-ASK NRZ format are also shown in Fig. 5(a)–(d) at respective points **a–d** in Fig. 3. As shown in Fig. 5(b)–(d), the harmonic generations are not that clearer in the RF spectra of NRZ formats compared with the corresponding RZ formats. This could be due to the fact that the average signal power requirement of NRZ is twice as large as RZ formats.

For the BER calculations, we used the lower eye-openings (as shown in Fig. 7) to calculate the SNR and later obtained the estimated BER from the SNR using the relations as follows [14]–[16]:

$$\text{SNR} = \frac{[\Re \times (P_{L_1} - P_{L_0})]^2}{(\sigma_0 + \sigma_1)^2} \tag{14}$$

$$\text{BER} = 0.5 erfc\left(\sqrt{\frac{\text{SNR}}{2}}\right). \tag{15}$$

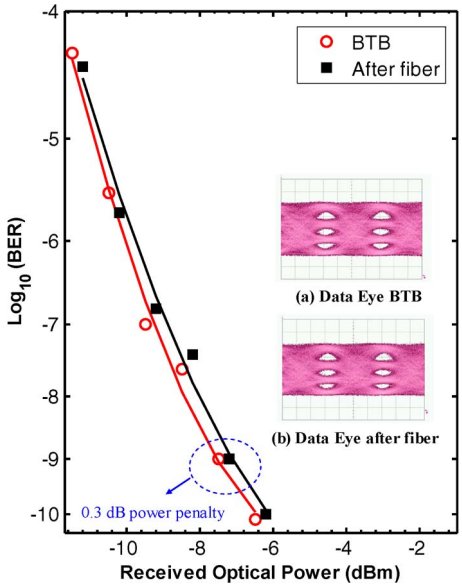

Fig. 8. Downlink BER curves and eye diagrams for scheme A using 4-ASK NRZ data.

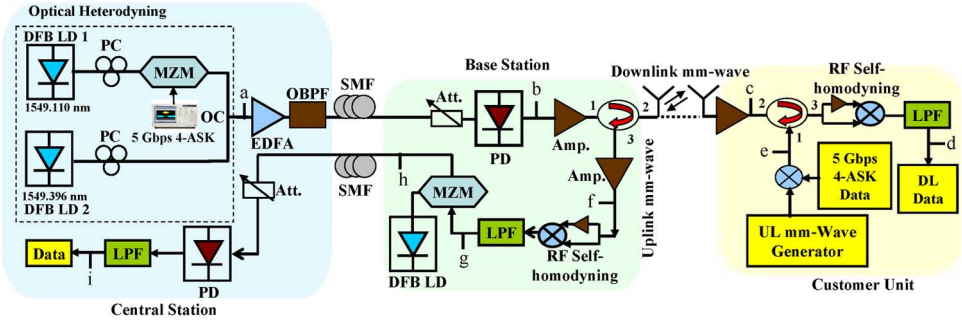

Fig. 9. Full-duplex system configuration for experimental demonstration of Scheme B.

Here, P_{L_1} and P_{L_0} are the power associated with logic 1 and logic 0. σ_0^2 and σ_1^2 are the noise variances of the signal and can be expressed as

$$\sigma_0^2 = P_{N_0} + NF_{AMP} + KTB_nNF_{RX} \tag{16}$$

$$\sigma_1^2 = P_{N_1} + NF_{AMP} + KTB_nNF_{RX}. \tag{17}$$

Here, P_{N_0} and P_{N_1} are the total noise of the PD using a Gaussian approximation including the shot noise variance components associated with P_{L_0} and P_{L_1}, respectively. Total noise in this case constitutes the thermal noise, shot noise, and relative intensity noise. NF_{AMP} and NF_{RX} are the noise figure of amplifiers and noise figure of the receiver, respectively. KTB_n is the thermal noise at the RF receiver, where K is the Boltzmann's constant, T is the temperature in Kelvin, and B_n is the noise bandwidth. An approximate effective SNR was calculated from the lower, middle, and upper eye openings using (14), and finally, a total BER was plotted for the received 4-ASK data.

Fig. 6 represents the downlink SNR for the lower eye openings at varying received optical power. For the error-free reception of data at a received optical power of -7 dBm, the SNR was found as 12.54 dB. This method calculates estimated SNR of the lower eye assuming that the noise distribution is Gaussian white. Additionally, eye openings for lower, middle, and upper eye are assumed be equal in our approximation, although lower eye will be exposed to higher noise floor.

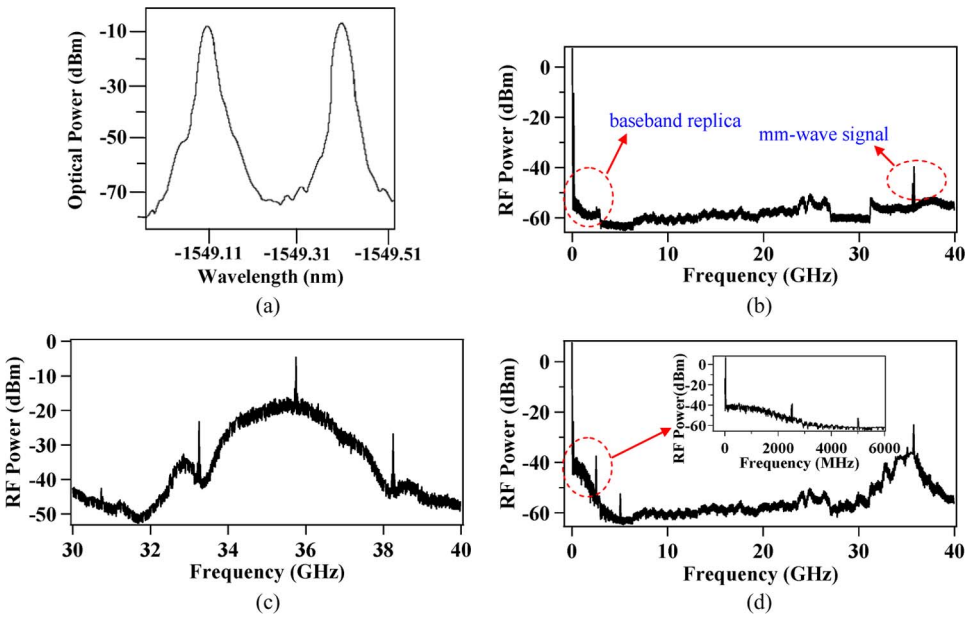

Fig. 10. (a)–(d): Optical and RF spectra at points a to d of the Scheme B using 4-ASK RZ data.

However, the estimated BER from (15) is not a very accurate approach as the ideal approximation might not be valid in all cases.

Fig. 7 therefore shows the estimated BER curves for the downlink experiments using RZ data (shown at the leftmost plots). At a BER of 10^{-9}, receiver sensitivity after SMF was found to be -10.1 dBm with negligible power penalty of 0.2 dB with respect to BTB. Hence, to further investigate the BER, we used a high-speed real-time oscilloscope where transmitted and received data sequences were captured and later compared through offline error counting to calculate the total BER. Fig. 7 also shows the calculated BER curves for the downlink experiments (shown in the middle plots). At a BER of 10^{-9}, receiver sensitivity after 25.1 km SMF was found to be -8.2 dBm. A negligible power penalty of 0.25 dB with respect to BTB was found in this case. For the downlink directions using RZ data, around 2 dB power differences in sensitivities is found between the estimated and calculated BERs. Therefore, except for the downlink and uplink 4-ASK RZ implementations in Scheme A; for the later BER calculations, we used BER measurements through offline error counting using a high-speed oscilloscope captured data sequence for better accuracy.

Fig. 8 presents the BER curves and eye diagrams for the downlink 5-Gb/s 4-ASK NRZ data. For an error-free BER at 10^{-9}, a receiver sensitivity of -7.1 dBm is found after the fiber transmissions. A power penalty of 0.3 dB was observed compared with BTB conditions.

3.2. 4-ASK Demonstrations Using Scheme B

3.2.1. Downlink

For Scheme-B demonstrations, DFB laser operating 1549.110 nm is modulated at the CS and later combined with the unmodulated DFB laser operating at 1549.396 nm. The rest of the setup is kept unchanged, as detailed in Section 3.1 and shown in Fig. 9. However, the power levels were controlled to manage equal power after the coupling of lasers.

3.2.2. Results and Discussion

Similar to Scheme A, relevant optical and RF spectra for downlink using 4-ASK NRZ format is shown in Fig. 10(a)–(d) at respective points a to d in Fig. 9. Similar optical and RF spectra were

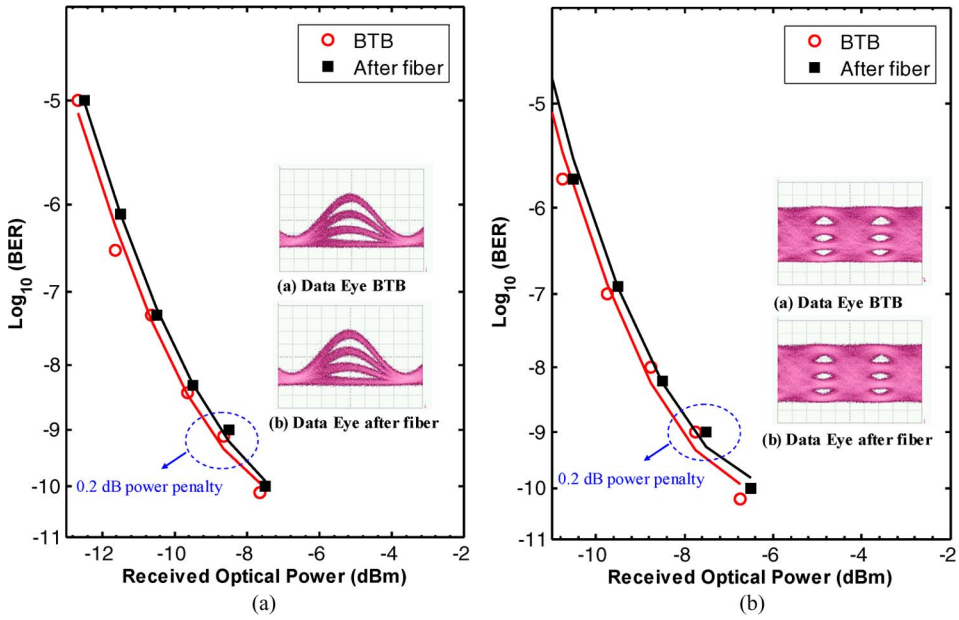

Fig. 11. BER curves and eye diagrams for downlink Scheme B using (a) 4-ASK RZ data and (b) 4-ASK NRZ data.

obtained for RZ 4-ASK data and is not hence shown in this paper. Fig. 11(a) shows the BER curves and eye-diagrams for the downlink 5-Gb/s 4-ASK RZ data. An error-free BER after the 25.1 km SMF transmissions can be found at a receiver sensitivity of −8.8 dBm. The power penalty compared with BTB conditions in such case was 0.2 dB. On the other hand, −7.8 dBm receiver sensitivity at an error-free BER for the same SMF transmissions was observed for the NRZ formats in Fig. 11(b). Minimal power penalty of 0.2 dB was found as well in this case.

3.3. 4-ASK Uplink Using Schemes A and B

For the uplink demonstration, an LO was used to generate mm-wave carrier at 35.75 GHz at the CU, as shown in Figs. 3 and 9. The generated and filtered 5-Gb/s 4-ASK data was then mixed with the 35.75 GHz mm-wave signal for upconversion. Both the NRZ and RZ formats were utilized in this case. Similar to downlink, the upconverted signal was amplified using a combination of LNA and MPA before RF self-homodyning at the BS. Necessary amplifications were provided at the LO port, and a Ka-band mm-wave phase shifter was used before the RF port to perform the RF-self homodyning using the *Miteq* Ka-band mixer. Due to RF self-homodyning, the data were retrieved at the BS. A DFB laser operating at 1549.15 nm was modulated by the downconverted data using 2.5 GHz MZM. The modulated signal was transmitted over a 25.1 km length of SMF and detected by a low-speed *Miteq* PD. The received data was filtered using suitable LPFs for both the NRZ and RZ formats.

3.4. Results and Discussions for 4-ASK Uplink

For the uplink 4-ASK RZ demonstrations, relevant optical and RF spectra are shown in Fig. 12(a)–(e) at respective points e to i in Figs. 3 and 9. Again, optical and RF spectra using 4-ASK NRZ data showed almost similar performance and is not hence shown in the paper. The upconverted mm-wave signal after the mixing of LO and 4-ASK data is shown in Fig. 12(a). The amplified version of the modulated mm-wave signal is presented in Fig. 12(b). RF spectra of the signal after the RF self-homodyning and filtering is shown in Fig. 12(c) with an inset of the retrieved data at BS. Fig. 12(d)

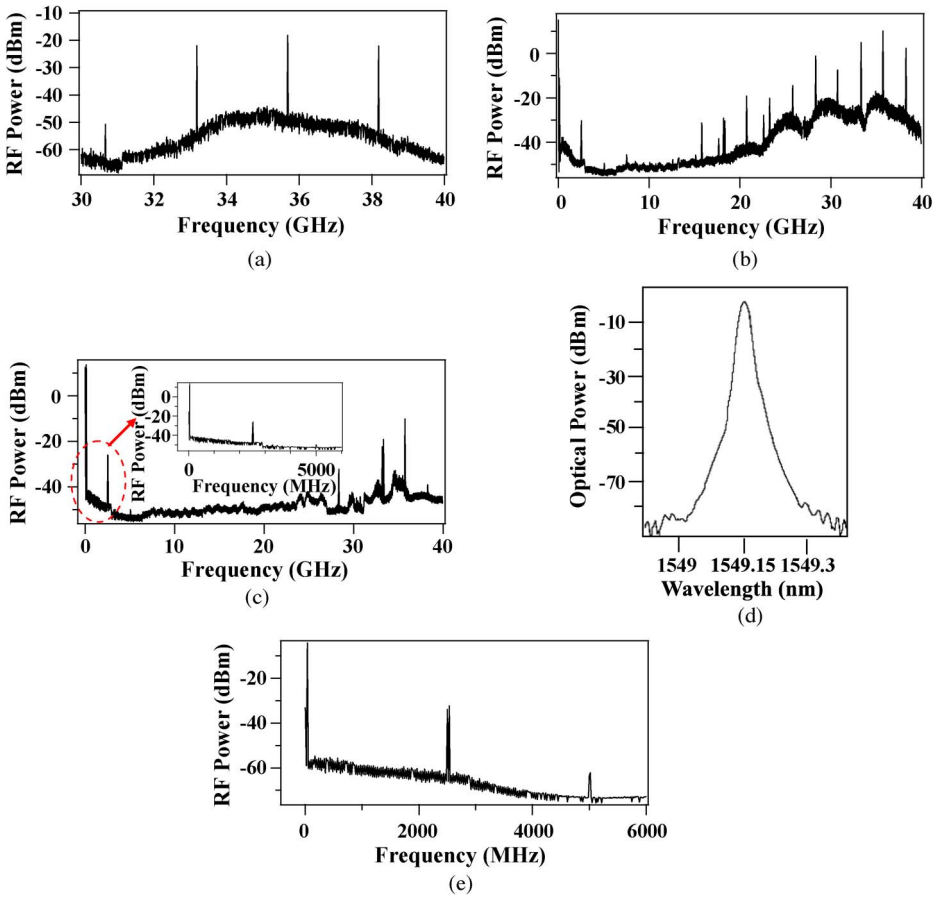

Fig. 12. (a)–(e): Optical and RF spectra for uplink using 4-ASK RZ data at respective locations e to i of the experimental setup shown in Figs. 3 and 9.

shows the modulated optical spectra at uplink prior to SMF transmission. The detected and filtered 4-ASK data are finally presented in Fig. 12(e).

Similarly, Fig. 13(a) shows the uplink BER curves and eye diagrams using 4-ASK RZ data. After the SMF transmissions, −11.1 dBm received sensitivity was found at an estimated BER of 10^{-9}. The power penalty in this case was 0.25 dB compared with BTB conditions. For the lower eye openings, a receiver sensitivity of −8.2 dBm is found for the same error-free BER. However, for the calculated BER through offline error counting using a high-speed oscilloscope data, we found a received sensitivity of −9.3 dBm at a BER of 10^{-9} with a power penalty of 0.3 dBm. Similar to downlink case, for the uplink directions using RZ data, around 2 dB difference in sensitivities is found between the estimated and calculated BERs. Hence, for better accuracy of BER calculation, Fig. 13(b) presents the calculated BER through offline error counting using a high-speed oscilloscope data along with the eye diagrams using 4-ASK NRZ data. In this case, error-free receiver sensitivity was found at −7.9 dBm after the SMF transmissions with a minimal power penalty of 0.25 dB.

3.5. 8-ASK Demonstrations Using Scheme A

3.5.1. Downlink

In order to examine even higher M-ASK signals such as 8-ASK, we utilized the downlink Scheme A experimental setup. Here, we generated 3.75 Gbps RZ 8-ASK data using the AWG for a data

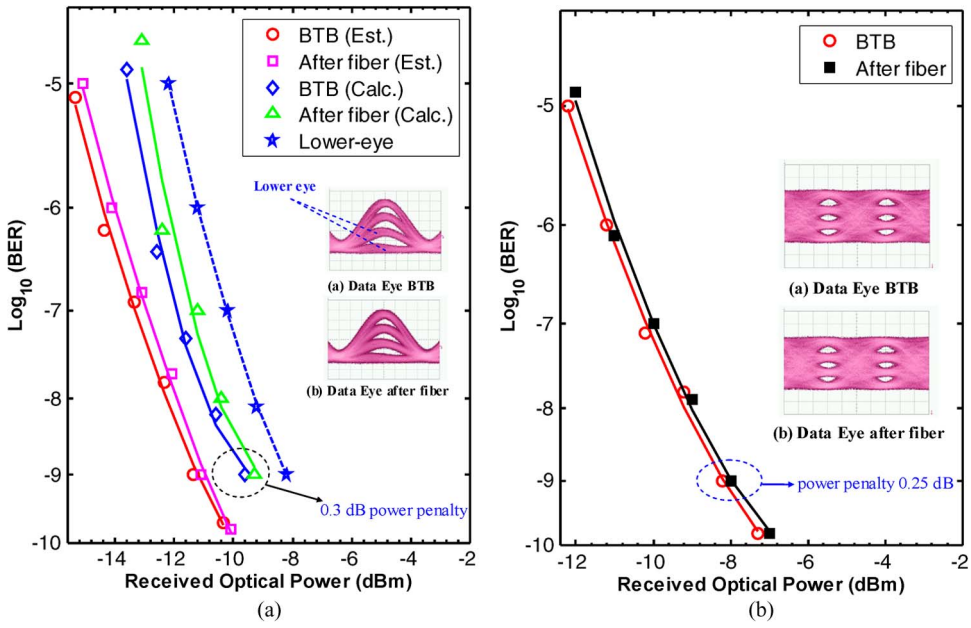

Fig. 13. Uplink BER curves and eye diagrams for Scheme A & B using (a) 4-ASK RZ data and (b) 4-ASK NRZ data.

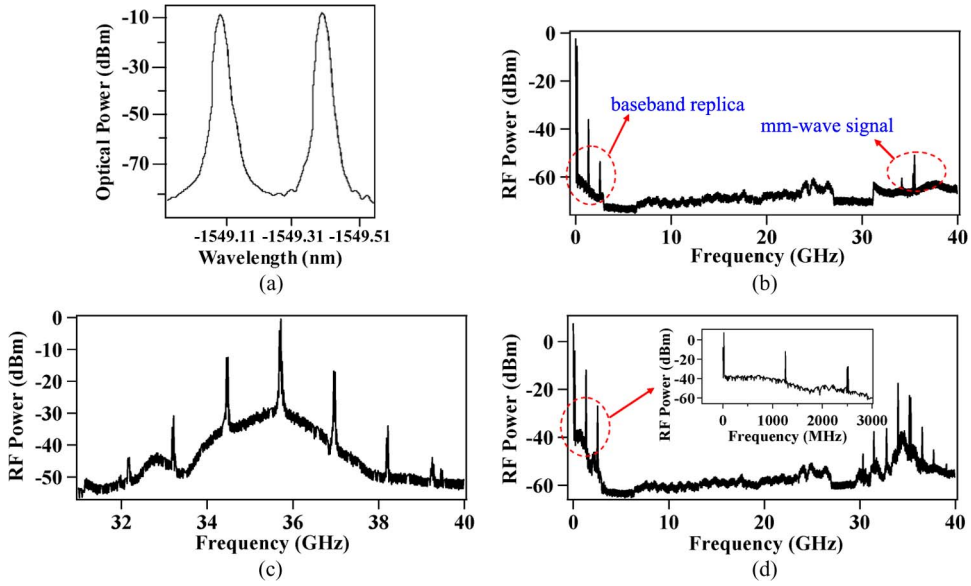

Fig. 14. (a)–(d): Downlink optical and RF spectra at points a to d of the Scheme A as in Fig. 3 using 8-ASK RZ data.

transmission bandwidth of 1.25 GHz. The sampling rate was 2.5 GS/s in this case. LPF of 2.5 GHz bandwidth was used in this experiment. Due to noisier performance of the NRZ format at 8-ASK, only RZ format was chosen for the 8-ASK experiments. The rest of the setup was unchanged and is not hence described here.

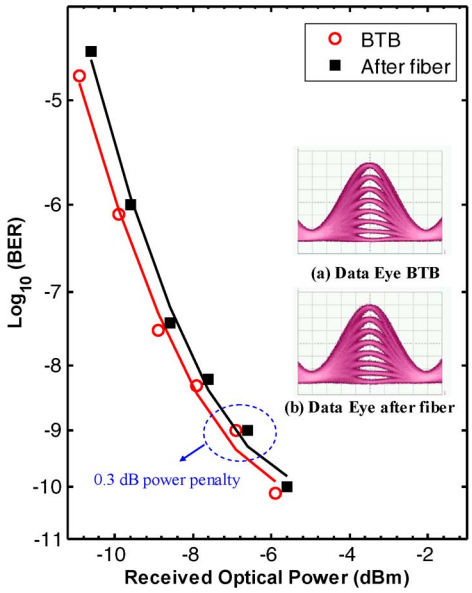

Fig. 15. BER curves and eye diagrams for downlink Scheme A using 8-ASK RZ data.

3.5.2. Results and Discussion

Like previous cases, relevant optical and RF spectra for the 8-ASK RZ implementations are shown in Fig. 14 at different points $\mathbf{a}$–$\mathbf{d}$ in Fig. 9.

The BER curves and relevant eye diagrams for this implementation are shown in Fig. 15. Error-free BER after SMF transmissions was found at a receiver sensitivity of -6.9 dBm in this case with a power penalty of 0.3 dB.

3.6. 8-ASK Uplink Using Scheme A

Similar to 4-ASK, 8-ASK RZ implementations were made for the uplink directions. The AWG sampling rate and LPF bandwidths were changed accordingly for this setup, as detailed in Section 3.5.1 for the downlink.

3.7. Results and Discussions for 8-ASK Uplink

For the uplink 8-ASK RZ demonstrations, Fig. 16(a)–(e) presents the relevant optical and RF spectra at respective points $\mathbf{a}$–$\mathbf{e}$ in Fig. 9. The BER curves and eye diagrams for this link is shown in Fig. 17. Receiver sensitivity of -7.7 dBm and a power penalty of 0.3 dB were observed in this case.

4. Discussions

The proposed M-ASK implementations for both downlink and uplink for phase-insensitive recovery of data have been demonstrated experimentally. From the signal generation point of view, both Scheme A and B exhibited almost similar performance using the respective formats. Schemes A and B were chosen being a perfect representation of spectrally efficient and dispersion tolerant OCS-DSB and OSSB+C modulation techniques [17]–[19]. In our demonstrations, receiver sensitivities in RZ formats showed better performance compared with the NRZ formats. This could be due to the fact that average signal power of NRZ is twice as large as the RZ signal. Also, power penalty was nominally identical after transmission through 25.1 km of SMF using both the NRZ and RZ formats, although RZ has better dispersion tolerance as compared with NRZ formats [20], [21]. Receiver sensitivities were relatively higher in our experimental implementations due to the higher input power requirements at the LO port of the high-speed mixer. A simple Schottky diode could replace such mixer, which does not need to be split for RF self-homodyning and thereby can avoid the extra input power needed for the LO port. While the receiver sensitivities are limited by the noise

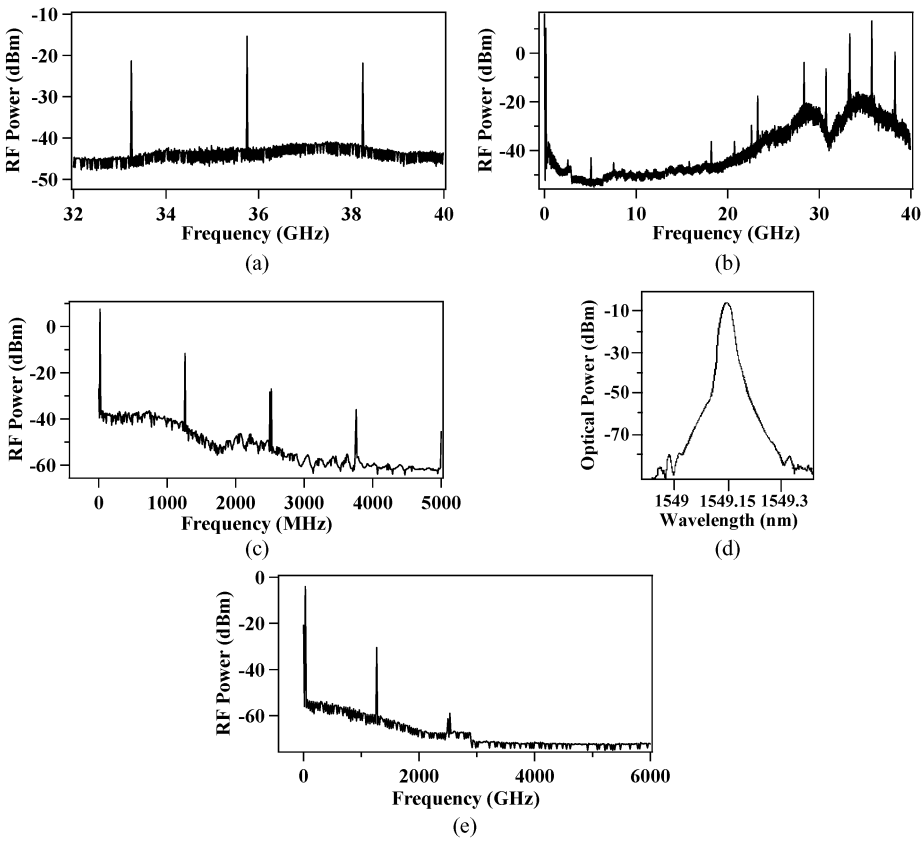

Fig. 16. (a)–(e): Optical and RF spectra at uplink using 8-ASK RZ data at locations e to i of the setup.

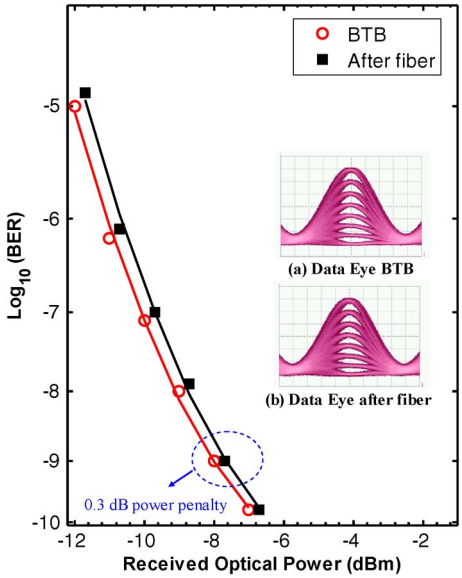

Fig. 17. BER curves and eye diagrams for uplink using 8-ASK RZ data.

levels of the M-ASK data, signal dependent noise arising from the square-law detection could lower the receiver sensitivity for even higher level M-ASK formats, and a tradeoff is therefore necessary between optimal spacing of amplitude levels and noise [22]–[24]. However, the M-ASK formats

introduced (using both NRZ and RZ formats) in the experiments reduce the bandwidth requirements of the transmitter and receiver by a factor of M compared with conventional ASK formats, thereby reducing the hardware complexity [25]–[27].

5. Conclusion

Proposed and demonstrated full-duplex signal generation schemes using multilevel 4-ASK and 8-ASK modulation formats confirm the phase-insensitive recovery of data for both downlink and uplink directions employing the unlocked optical heterodyning and RF self-homodyning. Although high-speed PD, LNA, MPA, and phase shifters are evident in our mm-wave RoF system, most of the high-speed electrooptic and RF device requirements such as high-speed LO, modulator, frequency/phase locking arrangements, etc., are eliminated using such technique. Data transmission efficiency has been also doubled or tripled without sacrificing the spectral bandwidth due to the introduction of M-ASK implementations in such systems. Therefore, considering low-cost optical mm-wave generation and transport, efficient frequency upconversion strategies, and simpler multilevel data transmission strategies, this kind of implementation can be a potential solution in offering multigigabit BWA services at a cheaper price to the consumers.

References

[1] A. Stöhr, "Multi-gigabit millimeterwave radio-over-fiber communication systems and networks," presented at the SPIE Photonics West, San Francisco, CA, Jan. 2012, paper 8282-13.
[2] M. Bakaul, A. Nirmalathas, C. Lim, D. Novak, and R. Waterhouse, "Simplified multiplexing scheme for wavelength-interleaved DWDM millimeter-wave fiber-radio systems," in *Proc. Eur. Conf. Opt. Commun.*, New York, 2005, pp. 809–810.
[3] Y. Li, A. Maedar, L. Fan, A. Nigam, and J. Chou, "Overview of femtocell support in advanced WiMAX systems," *IEEE Commun. Mag.*, vol. 49, no. 7, pp. 122–130, Jul. 2011.
[4] A. H. M. Razibul Islam, M. Bakaul, A. Nirmalathas, and G. Town, "Millimeter-wave radio-over-fiber system based on heterodyned unlocked light sources and self-homodyned RF receiver," *IEEE Photon. Technol. Lett.*, vol. 23, no. 8, pp. 459–461, Apr. 2011.
[5] A. H. M. Razibul Islam, M. Bakaul, A. Nirmalathas, and G. Town, "Simplification of millimeter-wave radio-over-fiber system employing heterodyning of uncorrelated optical carriers and self-homodyning of RF signal at the receiver," *Opt. Exp.*, vol. 20, no. 5, pp. 5707–5724, Feb. 2012.
[6] S. Walklin and J. Conradi, "Multilevel signaling for increasing the reach of 10-Gb/s lightwave systems," *J. Lightw. Technol.*, vol. 17, no. 11, pp. 2235–2248, Nov. 1999.
[7] J. M. Senior, *Optical Fiber Communications: Principles and Practice*. Englewood Cliffs, NJ: Prentice-Hall, 1992.
[8] L. N. Binh, B. Pujji, and S. L. Leong, "Vestigial side band (VSB) modulation formats for ultra-high capacity 40 Gb/s optical communications systems," Monash Univ., Melbourne, Australia, Tech. Rep. MECSE-24-2003, 2003.
[9] I. Garrett, D. J. Bond, J. B. Waite, D. S. L. Littis, and G. Jacobsen, "Impact of phase noise in weakly coherent systems: A new and accurate approach," *J. Lightw. Technol.*, vol. 8, no. 3, pp. 329–337, Mar. 1990.
[10] G. J. Foschini, L. J. Greenstein, and G. Vannucci, "Noncoherent detection of coherent lightwave signals corrupted by phase noise," *IEEE Trans. Commun.*, vol. 36, no. 3, pp. 309–314, Mar. 1988.
[11] I. Garrett and G. Jacobsen, "The effect of laser linewidth on coherent optical receivers with nonsynchronous demodulation," *J. Lightw. Technol.*, vol. 5, no. 4, pp. 551–560, Apr. 1987.
[12] R. S. Quimby, *Photonics and Lasers: An Introduction*. Hoboken, NJ: Wiley, 2006.
[13] C. P. Kaiser, M. Shafi, and P. J. Smith, "Analysis methods for optical heterodyne DPSK receivers corrupted by laser phase noise," *J. Lightw. Technol.*, vol. 11, no. 11, pp. 1820–1830, Nov. 1993.
[14] G. P. Agrawal, *Lightwave Technology Telecommunication Systems*. Hoboken, NJ: Wiley, 2005.
[15] F. Alsaadi and J. M. H. Elmirghani, "Adaptive mobile line strip multibeam MC-CDMA optical wireless system employing imaging detection in a real indoor environment," *IEEE J. Sel. Areas Commun.*, vol. 27, no. 9, pp. 1663–1675, Dec. 2009.
[16] N. S. Ribeiro, E. Conforti, and C. M. Gallep, "BER estimation from measured eye diagrams of a wavelength regenerative converter employing a single-SOA," in *Proc. Microw. Optoelectron. Conf.*, Nov. 2009, pp. 655–659.
[17] C. Lim, A. Nirmalathas, M. Bakaul, P. Gamage, K. Lee, Y. Yang, D. Novak, and R. Waterhouse, "Fiber-wireless networks and subsystem technologies," *J. Lightw. Technol.*, vol. 28, no. 4, pp. 390–405, Feb. 2010.
[18] G. H. Smith, D. Novak, and Z. Ahmed, "Overcoming chromatic dispersion effects in fiber-wireless systems incorporating external modulators," *IEEE Trans. Microw. Theory Tech.*, vol. 45, no. 8, pp. 1410–1415, Aug. 1997.
[19] A. Hilt, A. Vilcot, T. Berceli, T. Marozsak, and B. Cabon, "New carrier generation approach for fiber-radio systems to overcome chromatic dispersion problems," in *Proc. IEEE MTT-S*, Baltimore, MD, Jun. 1998, pp. 1525–1528.
[20] C. Fürst, G. Mohs, H. Geiger, and G. Fischer, "Performance limits of nonlinear RZ and NRZ coded transmission at 10 and 40 Gb/s on different fibers," in *Proc. OFC/NFOEC*, 2000, pp. 302–304.
[21] A. F. Judy, "Optimum fiber dispersion for multi-wavelength 40 Gbit/s NRZ and RZ transmission," in *Proc. ECOC*, Nice, France, 1999, vol. 2, pp. 280–281.

[22] J. Conradi, "Bandwidth-efficient modulation formats for digital fiber transmission systems," in *Optical Fiber Telecommunications IV B*, I. Kaminow and T. Li, Eds. New York: Academic, 2002, pp. 862–901.
[23] N. Avlonitis, "Multi-valued signalling for high efficiency optical communication systems," Ph.D. dissertation, Imperial College, Univ. London, London, U.K., Mar. 2005.
[24] G. A. Mahdiraji and A. F. Abas, "Advanced multiplexing techniques and modulation formats for optical communication systems," in *Trends in Telecommunications Technologies*. New York: In-Tech, 2009, pp. 1–26.
[25] D. Dahan, U. Mahlab, and D. Levy, "Novel all-optical quaternary amplitude shift keying modulation technique based on cross-gain modulation in a semiconductor optical amplifier," *Opt. Eng.*, vol. 48, no. 5, pp. 055007-1–055007-5, May 2009.
[26] N. Sotiropoulos, A. M. J. Koonen, and H. de Waardt, "Multi-level modulation formats for optical access networks," in *Proc. Symp. IEEE Photon. Benelux Chapter*, Brussels, Belgium, Nov. 2009, pp. 89–92.
[27] L. Huo, J. Zhao, C. Lin, C. Chan, and Z. Wang, "Experimental demonstration of a novel all-optical multilevel 4-amplitude-shifted-keying coding/decoding scheme," presented at the Optical Fiber Commun. Conf. Nat. Fiber Optic Eng. Conf., Santa Barbara, CA, Mar. 2006, paper JThB41.